Journal of Contaminant Hydrology 119 (2011) 1–12

Contents lists available at ScienceDirect

Journal of Contaminant Hydrology

journal homepage: www.elsevier.com/locate/jconhyd

# Impact of surfactant-induced wettability alterations on DNAPL invasion in quartz and iron oxide-coated sand systems

Ian L. Molnar *, Denis M. O'Carroll, Jason I. Gerhard

*Department of Civil and Environmental Engineering, The University of Western Ontario, London, ON, Canada N6A 5B9*

ARTICLE INFO

*Article history:*
Received 24 April 2010
Received in revised form 11 August 2010
Accepted 16 August 2010
Available online 21 August 2010

*Keywords:*
DNAPL
Wettability
Contact angle
Subsurface
Site remediation
Interfacial tension

ABSTRACT

Dense non-aqueous phase liquids (DNAPLs) present in the subsurface may contain surface active compounds that impact DNAPL migration and distribution. While a number of studies have revealed the role surface active compounds play in altering the wettability of quartz sand, few have considered the implications for other minerals common to contaminated sites. This study extends understanding of DNAPL/surfactant wettability to iron oxide surfaces. Specifically, quartz and iron oxide-coated sands in a tetrachloroethene (PCE)/water system containing the organic base (an organic molecule that acts as a base) dodecylamine (DDA) were compared at a variety of scales. Wettability of the minerals' surfaces, and the impact of wettability on capillary resistance to DNAPL entry, were assessed as a function of pH through: (i) advancing and receding contact angles, (ii) primary drainage capillary pressure–saturation experiments, and (iii) small, two-dimensional, flow cell experiments. The work revealed that, at neutral pH and under identical boundary capillary pressures, DNAPL invaded quartz sand but not iron oxide-coated sand; however, at low pH, DNAPL invaded both sands equally. These differences were demonstrated to be due to wettability alterations associated with the strength of attractive forces between DDA and the mineral surface, dictated by the isolectric point of the minerals and system pH. Observed differences in DNAPL invasion behavior were consistent with measured intrinsic contact angles and $P_c$–S relationships, the latter requiring scaling by the operative contact angle inside the porous medium for a meaningful comparison. This study suggests that the distribution of minerals (and, more specifically, their isoelectric points), as well as the aqueous phase pH at a given site, may have a significant impact on the DNAPL source zone architecture.



## 1. Introduction

Dense Non-Aqueous Phase Liquids (DNAPLs) released to the subsurface often pose a significant risk to the surrounding environment and populace. Although much effort has been made in recent years to limit the risks associated with DNAPL contaminated sites, a lack of knowledge in several key areas frequently hinders remediation efforts (National Research Council, 2005). One such area is the impact of wettability on DNAPL source zone architecture and remediation efficiency (Powers et al., 1996; Dwarakanath et al., 2002). Wettability is defined as the tendency of one fluid to preferentially spread over a solid surface in the presence of another fluid (National Research Council, 2005). For the purposes of this study 'wettability' refers to the contact angle ($\theta$) measured through the aqueous phase, 'advancing contact angle' refers to NAPL advancing over the solid surface and 'receding contact angle' refers to NAPL receding over the solid surface. A system with an advancing contact angle of $0° < \theta < 70°$ is typically considered water-wetting, $70° < \theta < 120°$ is intermediate wetting and $120° < \theta < 180°$ is NAPL-wetting (Powers et al., 1996).

The subsurface has been typically assumed to be water-wetting (Mayer and Hassanizadeh, 2005), where the aqueous phase preferentially coats the soil grains in the saturated zone

* Corresponding author. Fax: +1 519 661 3942.
*E-mail addresses:* imolnar@uwo.ca (I.L. Molnar), docarroll@eng.uwo.ca (D.M. O'Carroll), jgerhard@eng.uwo.ca (J.I. Gerhard).

0169-7722/$ – see front matter © 2010 Elsevier B.V. All rights reserved.
doi:10.1016/j.jconhyd.2010.08.004

and DNAPL occupies the larger pore bodies (Mayer and Hassanizadeh, 2005). However, intermediate and NAPL-wetting systems are not uncommon. For example, engineered wettability alterations in petroleum reservoirs are used to increase petroleum yield (Mercer and Cohen, 1990) and numerous coal tar and creosote contaminated sites have been identified as NAPL-wetting (Birak and Miller, 2009). In the laboratory, both neat solvents (Ryder and Demond, 2008) and solvents containing surface active chemicals have been demonstrated to act as the wetting fluid on quartz in the presence of water (Demond et al., 1994; Lord et al., 2000; Harrold et al., 2001, 2005; Hsu and Demond, 2007). Chlorinated solvents often contain surface active chemicals that improve their working efficiency (e.g., anti-oxidants and fabric softeners) and may also contain significant amounts of entrained grease, both of which may affect the solvent's interfacial properties (Jackson and Dwarakanath, 1999; Nellis et al., 2009; Yoon et al., 2009). Consequently, a variety of natural and anthropogenic surface active chemicals may be present in NAPLs at impacted sites (Jackson and Dwarakanath, 1999; Zheng et al., 2001; Dou et al., 2008; Nellis et al., 2009; Yoon et al., 2009). Under these circumstances, assuming a water–wet system may be inappropriate, with consequences including incorrect dissolution rate predictions (Bradford et al., 2000) or inaccurate conceptual models of fluid distribution potentially impacting remediation efficiency (e.g., waterflooding may be less effective than anticipated).

Considerable work has been completed studying the impact of typical NAPL constituents on wettability, in particular associated with crude oil/petroleum systems (Thomas et al., 1993; Powers and Tamblin, 1995; Buckley and Liu, 1998; Roy and McGill, 1998; Zheng and Powers, 1999; Buckley and Lord, 2003). In both the contaminated subsurface and petroleum reservoirs wettability alterations occur as a result of (i) precipitation of high molecular weight compounds onto the soil, and (ii) acid/base reactions between organic compounds and the electrical charge developed on the soil surface (Zheng et al., 2001). For example, Zheng and Powers (1999) correlated organic base concentrations in a variety of field NAPLs to soil wettability. At low pH, NAPLs with relatively high organic base concentrations preferentially wet quartz sand while NAPLs with low organic base concentrations did not wet the quartz sand.

Zheng and Powers (1999) postulated that pH was an important contributing factor to wettability alterations. At a sufficiently low pH, an organic base protonates, developing a positive charge (e.g., for dodecylamine (DDA) this occurs at pH 10.6). Meanwhile, as pH increases to the isoelectric point of the solid, the net surface charge of the solid surface transitions from positive to negative (Singh and Uehara, 1999). For example, quartz possesses a net negative charge above its isoelectric point at pH 2 (Sposito, 1989) and becomes increasingly negative as pH increases further. Thus, in the range $2<pH<10.6$, there is an electrostatic attraction between the negative quartz surface and positive charge of DDA. In general, wettability alterations are therefore expected for soils in the presence of NAPLs containing an organic base at pH values above the solid isoelectric point and below the pH at which the organic base loses its positive charge (Zheng and Powers, 1999).

A number of studies have focused specifically on wettability alterations related to surface active chemicals contained in chlorinated solvents (Demond et al., 1994; Powers and Tamblin, 1995; Powers et al., 1996; Lord et al., 1997, 2000; Harrold et al., 2001; Abriola et al., 2005; Harrold et al., 2005; Lord et al., 2005; Hsu and Demond, 2007). These results are consistent with the study of Zheng and Powers (1999) in that wettability alterations are functions of the concentration of cationic organic base in aqueous solution and the density of negatively charged sites on the solid surface. The concentration of cationic organic base in aqueous solution is, in turn, inversely proportional to the solution's pH. As the solution becomes more acidic, organic base will partition out of the NAPL and into the aqueous phase and will develop a predominantly cationic charge. This pH dependent partitioning is due to the higher aqueous solubility of the organic base when it possesses a cationic charge.

Most of the cited studies examined the wettability of solvents containing surface active chemicals with quartz as the solid surface. Although quartz is a very common subsurface material, there are many other typical subsurface minerals exhibiting different isoelectric points (Sposito, 1989) (Table 1). For example, the isoelectric point of hematite and goethite ranges between pH of 6 and 8, a substantially higher pH than quartz (Parks, 1965). Therefore, at neutral pH quartz is expected to exhibit a larger net negative surface charge than iron oxide. Organic bases, which are positively

**Table 1**
Common soil minerals and points of zero charge.

| Name | Ubiquity in Soils [a] | Environment [a] | Isoelectric Point |
|---|---|---|---|
| Quartz | Ubiquitous | Nearly all soils and parent materials | 2 [b] |
| Hematite and goethite | Ubiquitous | Well-drained, near surface soil | 6–10 [c] |
| Feldspars | Rare to common | Wide variety of igneous and metamorphic rocks | 2–2.4 [a] |
| Gibbsite | Common | Old, stable soils or feldspar pseudomorphs | 8–9 [a] |
| Kaolinite | Ubiquitous | Desilication of 2:1 lays/feldspathic | 4–5 [a] |
| Calcite | Common | Arid soils | 9.5 [a] |
| Hydroxy-interlayered vermiculite | Ubiquitous | Acid, highly weathered soil surface horizons | P [a,d] |
| Muscovite | Common | Granitic and high-grade metamorphic rocks | P [a,d] |

[a] (Feldman et al., 2008).
[b] (Cornell and Schwetmann, 2003).
[c] (Parks, 1965).
[d] Indicates that the soil maintains a permanent negative charge at all pH values.

charged at neutral pH, are thus expected to adsorb to quartz surfaces to a greater extent than iron oxide surfaces. As such, quartz surfaces are hypothesized to be less water-wetting relative to iron oxide surfaces in the presence of solvents containing an organic base at neutral pH. These minerals may have an impact that is disproportionately greater than their percentage of the total soil mass. A single sand grain will form a pore wall for several pores and can thus affect water drainage or imbibition behavior for numerous pores. Bauters et al. (2000) calculated that if only 3.1% of sand grains were hydrophobic then up to 37% of the pore spaces would have a pore wall that is hydrophobic.

The goal of this study was to determine the impact of DNAPL composition on surfactant-induced wettability alterations on quartz and iron oxide surfaces and to assess the impact of wettability alterations on DNAPL migration in soils containing these minerals. In particular, the role of mineral isoelectric point and surfactant charge on wettability alterations was examined for a dense chlorinated solvent, tetrachloroethene (PCE), containing DDA. First, the impact of pH on contact angle in a system containing PCE with DDA, water, and a surface of quartz or iron oxide was determined. Second, PCE/water primary drainage capillary pressure–saturation ($P_c$–S) relationships for quartz and iron oxide-coated sands in the presence of DDA at both low and neutral pH were measured. Third, the impact of pH on the migration of PCE/DDA in a small two-dimensional flow cell containing both quartz and iron oxide-coated sands was investigated. This methodology provided a link between wettability properties measured at the pore (contact angle) and representative elementary volume (REV) scales ($P_c$–S relationships) to DNAPL penetration into contrasting porous media.

## 2. Materials and methodology

### 2.1. Materials

The aqueous phase used throughout this study was distilled, deionized water (Milli-Q filters, Millipore, Billerica, Massachusetts). Aqueous phase ionic strength was controlled with NaCl (>99.5%) (Sigma-Aldrich, St. Louis, Missouri). The target aqueous phase pH was achieved using either HCl (Analytical Reagent grade, EML, Gibbstown, New Jersey) or NaOH (reagent grade pellets, Sigma-Aldrich, St. Louis, Missouri). The DNAPL employed was PCE (>99% purity, Acros Organics, Morris Plains, New Jersey) dyed with 0.01g/L Oil-Red-O (Fluka, St. Louis, Missouri ). Oil-Red-O was selected as it does not significantly impact interfacial properties at the concentration employed in this study (Jeong et al., 2002; Tuck et al., 2003). DDA (98% purity, Acros Organics, Morris Plains, New Jersey) was selected as the surface active chemical to facilitate comparison with literature studies (Lord et al., 2000, 2005; Hsu and Demond, 2007). DDA is a weak organic base in solution with a $pK_a$ of 10.6 (Lord et al., 2005). pH values were measured with a pH meter (Thermo-Scientific, Waltham, Massachusetts) accurate to +/−0.002 that was calibrated before each use with a three-point calibration curve.

Iron oxide was selected as the non-quartz surface in this study because of its ubiquity in the subsurface and its neutral to basic isoelectric point. Quartz and iron oxide slides (Alfa Aesa Ward Hill, Massachusetts) were used for contact angle quantification. XPS analysis of the iron oxide slides suggest a heterogeneous surface composed of both magnetite and hematite.

Flow cell and $P_c$–S experiments were performed with F-70 silica sand (U.S. Silica, Ottawa, Illinois). Iron oxide-coated F-70 sand was generated by thoroughly cleaning silica sand followed by overnight immersion in a 0.72M $FeCl_3$, pH 6.5 solution, then dried and heated overnight at 700 °C (Johnson et al., 1996). XPS analysis revealed that the coated sand surface was predominantly hematite and goethite. The isoelectric points for the iron oxide slides and iron-coated sand were estimated to be between pH 6.5 and 8 in contrast to pH 2 for the quartz slide and sand (Parks, 1965; Cornell and Schwetmann, 2003).

PCE/DDA/water mixtures were created using the same procedure for each set of experiments. DDA was added directly into the PCE phase in a flask containing a 1:6.3 volumetric ratio of PCE to water at $[DDA]_T = 0.0027$M. DDA speciation and distribution between the two fluid phases was governed by aqueous phase pH (Lord et al., 2000). $[DDA]_T$ is the concentration of DDA in the system normalized to aqueous phase volume (Lord et al., 2000):

$$[DDA]_\tau = \frac{(DDA)_{aq}V_{aq} + (DDA)_{org}V_{org}}{V_{aq}} \quad (1)$$

Where $(DDA)_{aq}$ and $(DDA)_{org}$ represent the concentration of DDA in the aqueous and organic phases, respectively. Likewise, $V_{aq}$ and $V_{org}$ are the volumes of the aqueous and organic phases, respectively. The aqueous phase of each mixture was titrated to the target pH in a stepwise manner. A known volume of 0.1 M HCl was added to the mixture and allowed to equilibrate for a 24-hour period on a vibrating table before the aqueous pH was measured. If the mixture had not reached its target pH then more HCl was added followed by another 24-hour equilibration period.

Particular attention was devoted to ensuring that all instruments, glassware and sand were free of impurities, particularly surfactant impurities that could affect interfacial properties. All glassware and instruments were cleaned prior to use with an established procedure (Lord et al., 2000). The quartz plates were cleaned in a similar manner to the glassware and, in addition, were soaked in 12 M HCl for 20 min and then rinsed with Milli-Q water. Metal columns, needle tips and iron plates were rinsed thoroughly with acetone and Milli-Q water. Sands were cleaned prior to use with a procedure similar to that employed by Johnson et al. (1996).

### 2.2. Interfacial tension and contact angle measurements

Interfacial tensions (pendant drop method with equilibrated water/PCE/DDA at target pH) and contact angles were measured using an Axisymmetric Drop-Shape Analysis (ADSA) system (First Ten Angstroms, Portsmouth, Virginia) (Lord et al., 2000). Contact angles were measured on the smooth quartz and iron oxide plates. The iron oxide plates, for the purpose of ensuring oxidation, were first immersed in a pH 13 solution and then heat treated at 500 °C for 12 h. Slides were equilibrated in the aqueous phase of the preequilibrated PCE/DDA/aqueous phase system for a minimum of 72 h. A

syringe, controlled by a stepping motor, slowly expelled or withdrew PCE onto the slide surface for advancing and receding contact angle measurements, respectively. For contact angle measurements, the needle tip remained just above the slide surface and inside the PCE drop to ensure stable, repeatable contact angle measurements. Digital photographs of the PCE droplet were recorded every 0.1 s as the droplet slowly advanced and receded over the slide facilitating contact angle quantification using ADSA software. At least 10 contact angle measurements were taken at different locations on the slide surface at each target pH to quantify spatial variability in contact angle on each slide surface.

### 2.3. Capillary pressure–saturation experiments

PCE/water primary drainage $P_c$–S relationships were quantified using the multistep outflow approach, a rapid and reliable method to quantify $P_c$–S relationships (O'Carroll et al., 2005b). This method employs a multiphase flow simulator coupled with an optimization routine to minimize the difference between observed and model cumulative water outflow by fitting van Genuchten $P_c$–S relationship parameters ($\alpha$, n and $S_{wr}$) (van Genuchten, 1980) and Brooks–Corey $P_c$–S relationship parameters ($P_d$, $\lambda$ and $S_{wr}$) (Brooks and Corey, 1964). The method was identical to the method outlined by O'Carroll et al. (2005b) with a few minor modifications: water pressure at the top column boundary was held constant by fixing the height of the outflow tube and PCE and aqueous phase pressures were measured using FP2000 pressure transducers (Honeywell) attached to the bottom and top of the column respectively. Also, the two transducers were fixed at the same height as the column. Multistep outflow experiments were performed at different aqueous phase pH values and with two different porous media types (Table 2). Dynamic effects in capillary pressure were not considered, since the method has been shown to provide a reliable estimate of $P_c$–S without incorporating them in similar circumstances (O'Carroll et al., 2005b).

### 2.4. Flow cell experiments

Flow cell experiments were conducted at pH 3.5 and pH 6.8 in a 5 cm × 5 cm × 1 cm thick aluminum flow cell with glass on the front and back face facilitating visualization via light transmission. This cell was previously employed for multiphase flow research (Gerhard and Kueper, 2003a,b) and was adapted for this work. The packing and saturation procedure was similar to that employed for the $P_c$–S experiments and is based on the procedure outlined in O'Carroll et al. (2005b). The flowcells and columns were drypacked with 1 cm lifts of sand, first flushed with $CO_2$ and then with 30 pore volumes of vacuum de-aired deionized water. However, here a specific packing was employed (Fig. 1) to allow side-by-side comparison of DNAPL penetration into both quartz and iron oxide-coated sands under identical boundary pressures and pH conditions.

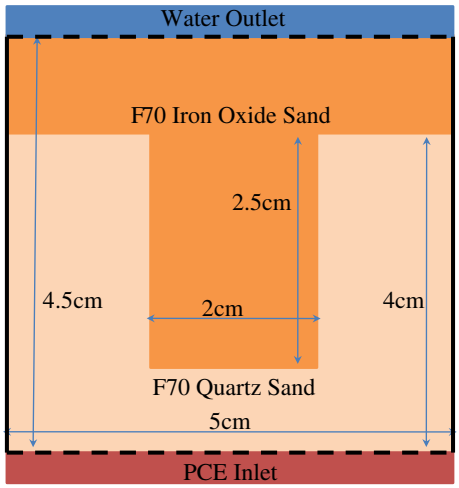


**Fig. 1.** The packing configuration of the flow cell. A T-shaped iron oxide heterogeneity was packed surrounded by a bed of quartz sand.

After dry packing the flow cell in compacted lifts, the cell was flushed with $CO_2$ and then slowly saturated with water. After achieving water saturation, the cell was left to sit for 12 h and was then flushed with aqueous solution that had equilibrated with the PCE/DDA mixture. Flushing continued until the influent and effluent aqueous phase surface tensions were within ±1 mN/m. Table 3 lists an overview of the experimental conditions for the flow cell experiments. While pH values for the $P_c$–S (Table 2) and flow cell experiments (Table 3) are not identical (due to the challenge of fixing pH) they are similar enough to permit meaningful comparisons.

The top of the flow cell was connected to water-filled tubing terminating at a set height and open to the atmosphere to control the aqueous phase pressure. The bottom of the flow cell was attached to a PCE reservoir that could be raised to control the DNAPL pressure. The height of the PCE reservoir was increased in approximately 0.5 cm increments and the DNAPL height in the flow cell was allowed to reach equilibrium between each invasion step. The system was considered to have reached equilibrium if no additional advancement of the hydrostatic DNAPL surface within the flow cell occurred after 30 min.

Light transmission visualization (LTV) was used to track PCE/water flow in the two-dimensional flow cell (Niemet and Selker, 2001). A digital CCD camera (Nikon D80 with Nikkor 35–75 mm lens) was used to photograph the cell at

**Table 2**
Capillary pressure–saturation experiments.

| pH | Sand type | Porosity | IFT (mN/m) |
|---|---|---|---|
| NA | Quartz, no DDA present | 0.29 | 47.1 |
| 3.2 | Quartz | 0.34 | 6.99 |
| 3.6 | Iron oxide-coated | 0.34 | 6.06 |
| 6.3 | Quartz | 0.34 | 14.4 |
| 6.3 | Iron oxide-coated | 0.33 | 14.4 |

**Table 3**
Flow cell experimental conditions.

| pH | IFT (mN/m) | Porosity |
|---|---|---|
| 3.5 | 9.9 | 0.31 |
| 6.8 | 19 | 0.33 |

predefined intervals. A camera flash (Nikon SB800) was employed as the light source at the back of the cell, and was triggered automatically by the camera for each photograph. This setup was selected, in part, to avoid temperature changes often associated with the use of a light bank. The experiment took place in a dark room to eliminate variations in the background light and the flash was shuttered so that all of the light passed through the apparatus. The consistency of the flash output intensity was measured over time in a sand/water flowcell and the variation in output intensity was found to be much less than the drop in light intensity as NAPL imbibes into the sand.

Studies have tracked DNAPL migration by measuring changes in hue (Darnault et al., 1998; O'Carroll et al., 2004), changes in colour saturation (Gerhard and Kueper, 2003a) and changes in light intensity (Niemet and Selker, 2001; McNeil et al., 2006; O'Carroll and Sleep, 2007; Bob et al., 2008; Wang et al., 2008). In this work, the objective was to compare the extent of PCE invasion in the quartz sand and iron oxide-coated sand. MATLAB was used to quantify light intensity reduction at a given pixel due to NAPL invasion at that pixel. The images were captured in an sRGB colorspace and converted to light intensity ($I$) (Stokes et al., 1996):

$$I = 0.2126R + 0.7152G + 0.0722B \quad (2)$$

Grant et al. (2007) demonstrated that a similar technique successfully tracked the evolution of DNAPL presence in a heterogeneous porous media experiment.

## 3. Results and discussion

### 3.1. Contact angle and interfacial tension

Contact angles were measured on smooth quartz and iron oxide slides for $3.2<pH<7.5$ and $[DDA]_T = 0.0027M$ to assess the impact of surface charge and surfactant [DDA] on wettability. Contact angles were not measured above a pH of 7.5 in order to avoid the competing effects of an increasingly negative surface charge and decreasing cationic [DDA]. This pH range captures the majority of the difference in the isoelectric points of quartz (pH 2) and iron oxide (pH 6–9) (Parks, 1965). Fig. 2 provides representative ADSA images: at pH 6.5, the quartz surface was highly hydrophobic ($\theta_A = 160°$) while the iron oxide plate remained strongly hydrophilic ($\theta_A = 24°$). Measurements of advancing contact angle at a variety of locations on both the quartz and iron oxide-coated surfaces yielded similar results.

The PCE advancing contact angle ($\theta_A$) on quartz was a strong function of pH at $[DDA]_T = 0.0027$ M (Fig. 3). In Fig. 3, the mean of all advancing contact angles (minimum of 10) measured at a single pH, along with the 95% confidence intervals, are plotted as a function of pH. The calculated mean combines multiple PCE droplets at a single pH (minimum of 2 droplets per data point) as well as multiple advances of a single droplet (minimum 5 advances per data point). At low pH, the quartz remained strongly hydrophilic with an average value of 24° at pH 3.7. Due to the small net negative surface charge of quartz at this low pH, it is expected that only a relatively minor amount of the cationic DDA sorbed to the quartz surface despite an abundance of DDA in solution. With increasing pH, the quartz surface became NAPL-wetting with a maximum contact angle of 158° at pH 6.2 (Fig. 3). This is likely an optimal system point where the cationic DDA concentration is at solubility in the aqueous phase ($1\times10^{-3}$ M) and the quartz has a strong net negative charge. Above pH 6.5, there was an increased variability in measured advancing contact angles on quartz with a trend of decreasing contact angle with pH with some values in the intermediate wettability range. As pH increases, a greater amount of DDA partitions into the organic phase resulting in relatively less (and more irregularly distributed) DDA on the quartz. However, these mechanisms may not be the only cause of variability. It is worth noting that Lord et al. (2000) observed more scatter in their contact angle measurements across all pH values, likely due in part to the lower DDA concentration employed in their study ($[DDA]_T = 0.001$ M). Overall, the advancing contact angle trends measured on the quartz plate are consistent with previous studies involving DDA (Lord et al., 2000, 2005; Hsu and Demond, 2007).

In contrast to the results for quartz, PCE advancing contact angles on the iron oxide surface suggest that the surface is hydrophilic throughout the entire pH range in the presence of DDA (Fig. 3). The maximum difference in the advancing contact angles measured on the two surfaces was 130° at pH 6.5, with the iron oxide surface being hydrophilic ($\theta_A = 25°$)

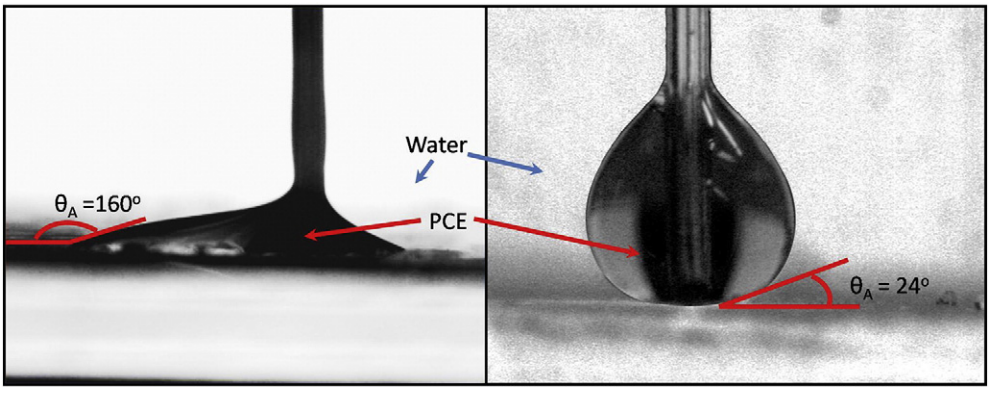


**Fig. 2.** PCE droplets advancing over quartz (left image) and iron oxide surfaces (right image) immersed in water at pH 6.5. The needle tip was left in the PCE droplet during imaging. $[DDA]_T = 0.0027M$.

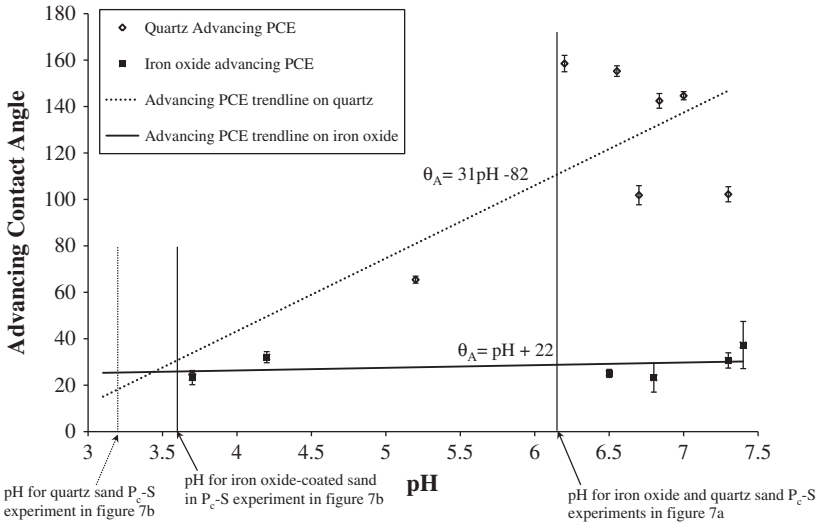


**Fig. 3.** Advancing contact angle versus pH for PCE on quartz and iron oxide surfaces as measured through the water phase with $[DDA]_T = 0.0027M$. Each symbol represents the mean of at least 10 measurements and is presented with its associated 95% confidence interval (where it is not visible, the interval is smaller than the symbol dimensions). Best fit linear regression trendlines for contact angles measured on quartz and iron oxides are overlain as are lines indicating the pH at which specific $P_c$–S (multistep outflow) experiments were conducted.

while the quartz surface was hydrophobic ($\theta_A = 155°$) under identical conditions. In this pH range both the iron oxide plate and DDA are positively charged, thus no sorption of DDA on the plate is expected. This explanation is supported by the fact that contact angles on iron oxide measured in the presence of DDA were indistinguishable from those measured for the same system in the absence of DDA (figure not shown).

As suggested by previous studies (Murray and Darvell, 1990; Sghaier et al., 2006; Arye et al., 2007) the data of Fig. 3 is plotted with the cosine of the contact angle as the dependent variable in Fig. 4. The figure underscores that the sensitivity of displacement pressure ($P_D$) to pH is expected to solely be a function of interfacial tension for the iron oxide sand whereas the sensitivity of $P_D$ to pH for quartz sand is expected to be a function of both interfacial tension and contact angle. Negative $\cos(\theta_A)$ implies spontaneous imbibition of NAPL; however, as discussed below, the intrinsic contact angle measured on a smooth plate is often greater than the operative contact angle in a porous medium. This phenomenon has been traditionally associated with the roughness and geometry of the porous medium (Morrow, 1975).

Interfacial tension (IFT) of the PCE/water/DDA systems was a function of pH (Fig. 5). Interfacial tension values are reported as a mean value in pH intervals of 0.5 accompanied by the 95% confidence interval if more than 3 droplets with 10 measurement images were recorded in that 0.5 pH interval. PCE/water IFT in the absence of DDA was measured to be 47 mN/m. Lord et al. (2005), employing 2.7 times less $[DDA]_T$

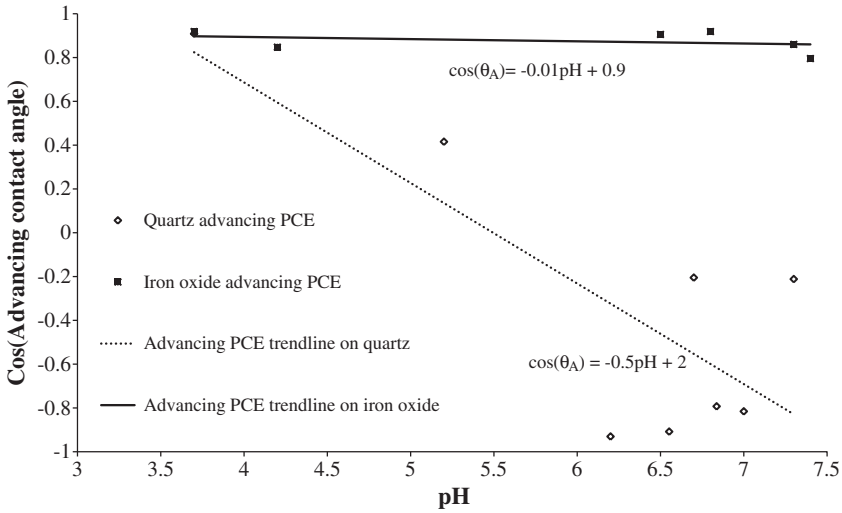


**Fig. 4.** Advancing cos(θ) versus pH for PCE on quartz and iron oxide surfaces as measured through the water phase with $[DDA]_T = 0.0027M$. Each symbol represents the mean of at least 10 measurements. Best fit linear regression trendlines for $\cos(\theta_A)$ measured on quartz and iron oxides are overlain.

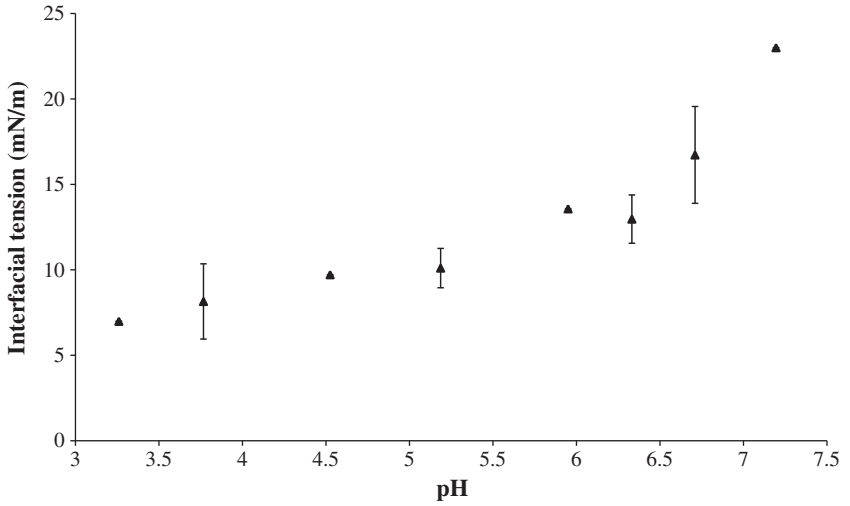


**Fig. 5.** Averaged interfacial tension measurements versus pH for PCE/water/DDA with $[DDA]_T = 0.0027M$.

than this study, found that IFT reached a minimum of approximately 20 mN/m at pH<5, and attributed the IFT reduction to the accumulation of DDA at the NAPL/water interface. Fig. 5 reveals a two-stage IFT reduction with pH. First, IFT decreased rapidly from 23 mN/m at pH 7.2 to 13 mN/m at pH 6.3, which is expected due to the partitioning of DDA from the organic phase into the aqueous phase until it reached solubility in latter (Lord et al., 2005). Second, IFT decreased slowly to a minimum of 6.5 mN/m at pH 3.2; this is expected because, although the DDA should be at solubility in the aqueous phase, continued increase in DDA interfacial activity has been reported with decreasing pH (Lord et al., 2005; Hsu and Demond, 2007).

PCE receding contact angles ($\theta_R$) were also quantified over the same pH range (Fig. 6). Above pH 6, quartz was so hydrophobic that PCE would not recede from the surface; instead a thin PCE film remained on the quartz surface after the droplet was retracted. Therefore, above pH 6 the receding contact angle on quartz is reported as 180°.

Hysteresis of contact angle was observed on the quartz surface with $\theta_R > \theta_A$ over the evaluated pH range (Figs. 3, 6). These figures reveal negligible hysteresis on the iron oxide surface for 3.7<pH<6.3. However, $\theta_R$ increases sharply from 27° at pH 6.5 to 126° at pH 6.8 as the system transitions through the iron oxide isoelectric point. At pH 7.4, PCE would not retract from the iron oxide surface, representing strong hydrophobic behavior similar to that observed for quartz at pH 6. While the maximum magnitude of the $\theta$ hysteresis (83° at pH 7.3) was expected for quartz (Desai et al., 1992), the even greater $\theta$ hysteresis for iron oxide at neutral pH (142°) has not been previously reported.

### 3.2. Capillary pressure–saturation

Aqueous phase/PCE ($[DDA]_T = 0.0027M$) van Genuchten and Brooks–Corey $P_c$–S relationships were quantified using a multistep outflow approach (O'Carroll et al., 2005b) for quartz and oxide-coated sand at pH $3.4 \pm 0.2$ and pH 6.3 (Table 4). As presented in Fig. 7a (Brooks–Corey curves not

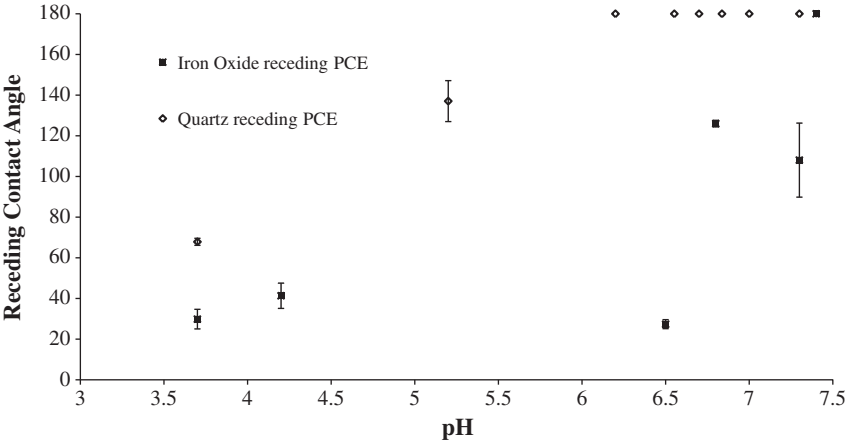


**Fig. 6.** Contact angles of PCE receding over quartz and iron oxide surfaces as measured through the water phase as a function of pH. [DDA]T = 0.0027M. Where possible, error bars representing 95% confidence intervals are shown.

**Table 4**
Best fit parameters for $P_c$–S experiments[a].

| pH | Sand type | van Genuchten parameters | | Brooks–Corey parameters | |
|---|---|---|---|---|---|
| | | α (1/cm) | n | $P_D$ (cm $H_2O$) | λ |
| 3.2 | Quartz | 0.22 (0.21–0.22) | 4.5 (4.2–4.9) | 3.5 (3.4–3.7) | 1.7 (1.4–2.0) |
| 3.6 | Iron oxide-coated | 0.26 (0.22–0.30) | 3.4 (2.7–4.0) | 2.7 (2.5–2.9) | 0.81 (0.63–0.95) |
| 6.3 | Quartz | 0.23 (0.20–0.26) | 3.4 (2.9–3.9) | 4.9 (4.5–5.3) | 2.6 (1.8–3.3) |
| 6.3 | Iron oxide-coated | 0.11 (0.10–0.11) | 4.5 (4.3–4.8) | 6.8 (6.6–7.0) | 1.5 (1.3–1.7) |

[a] 95% confidence intervals (generated by the LM-OPT inverse modeling package) presented in parenthesis.

shown), primary drainage capillary pressures in the iron oxide system at pH 6.3 were approximately double those in the quartz system. For example, at 50% effective water saturation capillary pressure was 5 cm and 10 cm water in the quartz sand and iron oxide sand systems, respectively (Fig. 7a). However the $P_c$–S relationships obtained for the quartz and iron oxide systems at pH 3.4 ± 0.2 were similar, with a capillary pressure of approximately 5 cm water at 50% water saturation (Fig. 7b). This general trend with pH is consistent with contact angle measurements: at pH 6.3, larger $\theta_A$ on the quartz surface, in comparison to the iron oxide surface, corresponds to reduced primary drainage $P_c$, while at pH 3.4, similar $\theta_A$ measurements for both quartz and iron oxide surfaces correspond to similar $P_c$–S relationships. At pH

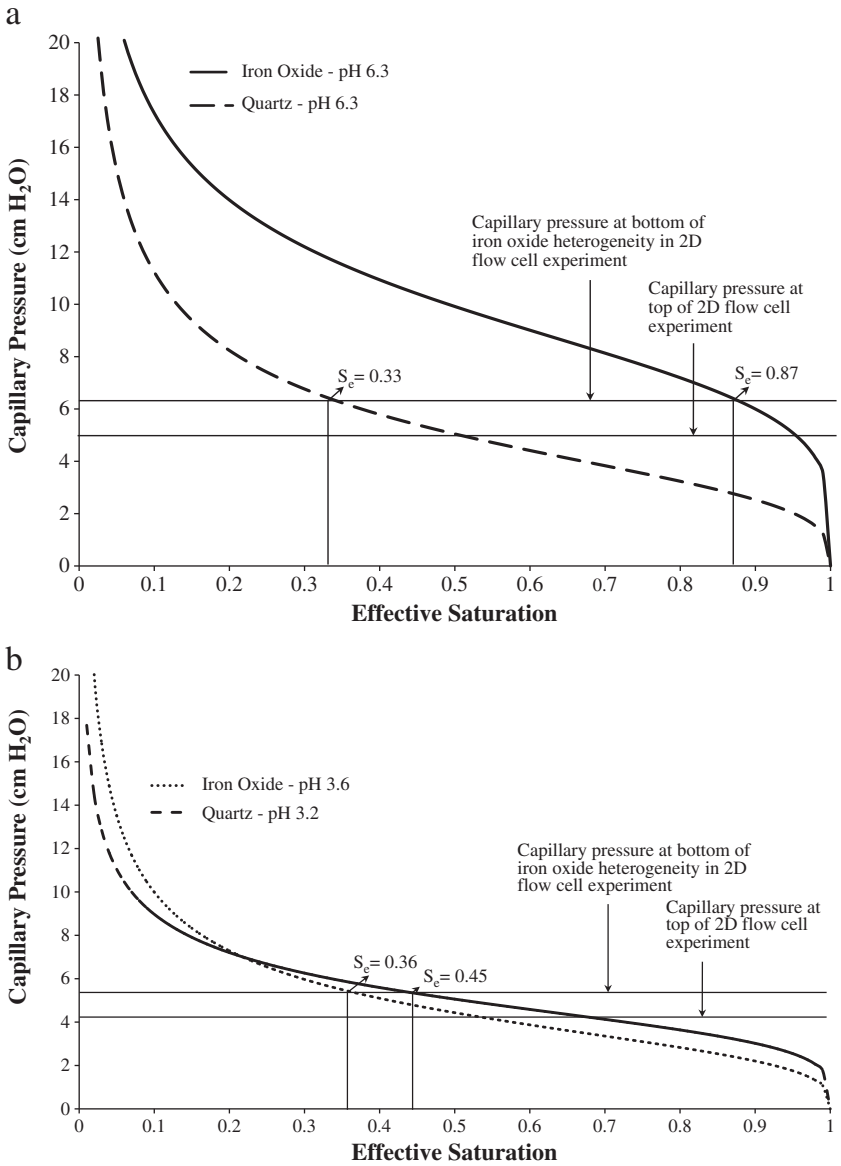


**Fig. 7.** van Genuchten $P_c$–S relationships for quartz and iron oxide-coated sands at a pH of 6.3 (a) and 3.2/3.6 (b) where $[DDA]_T = 0.0027M$. Overlain are lines representing the capillary pressure at the bottom of the iron oxide-coated heterogeneity and at the top of the flow cell for the images shown in Fig. 9. Also shown are the estimated effective water saturations for the quartz and iron oxide-coated sands at the bottom of the heterogeneity.

6.3 measured IFTs were identical and at the lower pH measured IFTs were similar (Table 5). As such, reported differences in $P_c$–S curves are due to wettability differences. To further illustrate the correspondence between intrinsic contact angles measured on smooth slides and primary drainage $P_c$–S curves, pH values at which the $P_c$–S experiments were conducted are indicated on Fig. 3.

Previous studies have suggested that (intrinsic) contact angles measured on smooth surfaces (through the aqueous phase) are typically larger than (operative) contact angles in porous media systems (Morrow, 1975; Desai et al., 1992; O'Carroll et al., 2005a). The wettability-modified Leverett scaling approach was employed to estimate contact angle in the porous media systems (Desai et al., 1992; Demond et al., 1994) for comparison with the intrinsic contact angle:

$$P_{c2}(S_\theta)_2 = P_{c1}(S_\theta)_1 \frac{(\gamma_2 cos\theta_o Z(\theta_o))_2}{(\gamma_1 cos\theta_o Z(\theta_o))_1} \quad (3)$$

where subscripts 1 and 2 refer to fluid–fluid–solid systems 1 and 2, respectively, $P_c$ is capillary pressure, $S_e$ is effective saturation, $\gamma$ is interfacial tension, $Z(\theta_o)$ is the curvature correction factor, and $\theta_o$ is the operative contact angle. The curvature correction function was introduced by Melrose (1965) to account for the influence of pore geometry on contact angles observed in a capillary tube and was quantified in this study with the formulae given in Melrose (1965). $\theta_{o,}$ was introduced by Morrow (1975) to represent the influence of roughness on $\theta_{int}$, the intrinsic contact angle. Based on results from a series of capillary tube experiments with surfaces of varying wettability, Morrow (1975) proposed:

$$\theta_o = 0°, \quad 0° < \theta_{int} < 21.6° \quad (4a)$$

$$\theta_o = 0.5 exp\,(0.05\theta_{int}) - 1.5, \quad 21.6° < \theta_{int} < 87.6° \quad (4b)$$

For the two low pH $P_c$–S experiments and for the pH 6.3 iron oxide-coated sand $P_c$–S experiment $\theta_o$ was estimated to be <1° using Eq. (4b) (Table 5). In these systems the $\theta_{int}$ values, independently quantified using the ADSA approach, were very close to 21.6°, the upper limit of applicability for Eq. (4a), resulting in small operative contact angles (i.e., strongly water-wetting). For the quartz sand $P_c$–S experiment at pH 6.3, $\theta_o$ was estimated to be 61° and 63° for the van Genuchten and Brooks–Corey fits, respectively; because $\theta_{int}$, (160°) was outside of the applicability limits of Eq. (4b), the estimate was obtained via Eq. (3) by minimizing the root sum of squared difference between the quartz and iron oxide $P_c$–S curves at pH 6.3. Although the operative contact angle is smaller, $\cos(\theta_o)$ for this system is approximately 0.5, suggesting that wettability corrections are important in estimating the $P_c$–S relationship.

To assess the appropriateness of this scaling approach, all of the measured $P_c$–S relationships were normalized by dividing the measured capillary pressure by the measured interfacial tension and cosine of the operative contact angle (Fig. 8). Scaling based solely on IFT was a reasonable assumption for the iron oxide pH 6.3 system and the quartz and iron oxide sands at pH $3.4 \pm 0.2$ systems. However, wettability corrections are required to achieve good agreement between the other three $P_c$–S curves and the quartz sand pH 6.3 $P_c$–S curve. Of the two modifications, it is noted that the curvature correction, $Z(\theta_o)$, accounts for 23% of the scaling and wettability, $\cos(\theta_o)$, accounts for 76% of the scaling. In summary, the van Genuchten and Brooks–Corey results from the $P_c$–S experiments are consistent with expectations based upon intrinsic contact angle measurements.

### 3.3. Flow cell experiment

Two flow cell experiments were conducted at low and neutral pH values (3.5 and 6.8, respectively) to evaluate if smooth slide and $P_c$–S curve results are consistent with DNAPL invasion observed in a simple heterogeneous system with quartz and iron oxide-coated sand. Sand and fluid pair systems were identical in these experiments to those in the $P_c$–S experiments except that, in the latter, each sandpack was distinct and homogeneous while, in the flow cell, an iron oxide heterogeneity was embedded within quartz sand (Fig. 1).

In the neutral pH experiment (pH 6.8), PCE invaded upward, initially displacing water from the quartz sand at the base of the flow cell. However, when PCE reached the base of the iron oxide-coated sand heterogeneity it did not enter and instead continued to migrate upwards on either side of the heterogeneity. As such, PCE did not enter the iron oxide-coated sand but did enter the quartz sand at identically applied capillary pressures (Fig. 9a); this result from the LTV analysis was confirmed with destructive sampling. This behavior is consistent with differences in measured $P_c$–S curves (Fig. 7a) as well as observed differences in intrinsic contact angle (Fig. 3).

In the pH 3.5 flow cell experiment PCE initially invaded in a similar manner to the neutral pH experiment. However, when PCE reached the base of the iron oxide-coated sand heterogeneity it displaced water from the iron oxide-coated sand, and adjacent quartz sand, at approximately the same rate (results not shown). That is, there was no observable temporal lag between PCE invading quartz sand and iron oxide-coated sand pores, at similar capillary pressure

**Table 5**
IFT, intrinsic and fit operative contact angles for $P_c$–S experiments.

| pH | Sand type | Interfacial tension (mN/m) | Intrinsic contact angle (°) | van Genuchten operative contact angle fitting | | Brooks–Corey operative contact angle fitting | |
|---|---|---|---|---|---|---|---|
| | | | | Operative contact angle(°) | Curvature correction | Operative contact angle(°) | Curvature correction |
| 3.2 | Quartz | 6.9 | 23 | <1 | 0.938 | <1 | 0.938 |
| 3.6 | Iron oxide-coated | 6.1 | 24 | <1 | 0.938 | <1 | 0.938 |
| 6.3 | Quartz | 14 | 160 | 61 | 1.17 | 63 | 1.23 |
| 6.3 | Iron oxide-coated | 14 | 25 | <1 | 0.938 | <1 | 0.938 |

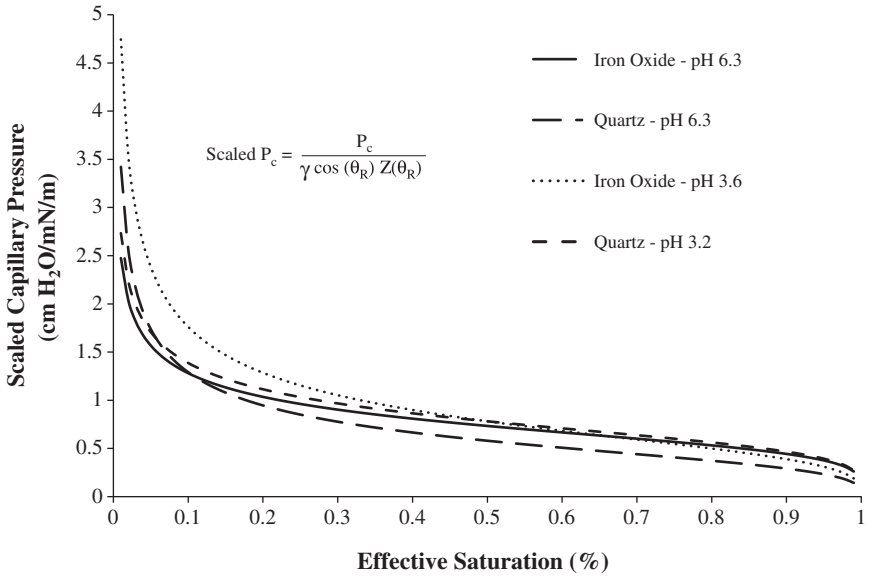


**Fig. 8.** Primary drainage van Genuchten $P_c$–S relationships scaled using equation displayed in figure with relevant van Genuchten and Brooks–Corey parameters listed in Tables 4 and 5. $[DDA]_T = 0.0027M$.

conditions. This behavior is consistent with expected behavior based on measured $P_c$–S curves (Fig. 7b) as well as with measured intrinsic contact angles (Fig. 3). These results also suggest that the relative permeability relationships are similar in both sands, as expected, since both sands have the same grain size distribution and wetting condition. At the completion of this flow cell experiment LTV analysis and subsequent destructive sampling suggest that PCE was distributed equally throughout both sands (Fig. 9b).

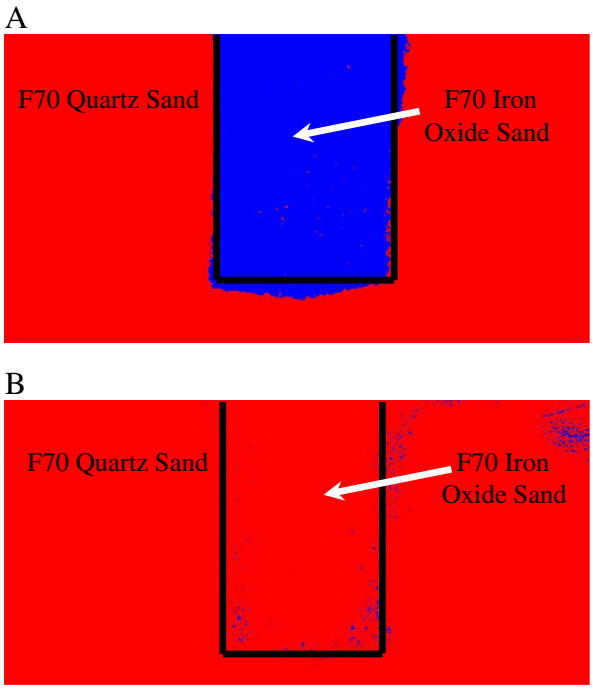


**Fig. 9.** Fluid distributions in flow cell experiments for pH 6.8 (a) and pH 3.5 (b) pH. In a and b, red represents PCE saturated porous media and blue represents water saturated porous media. The approximate location of the iron oxide-coated sand heterogeneity is overlain on the images for ease of interpretation. For image a, $P_c$ at the base of the pH 3.5 sandbox = 9.9 cm $H_2O$, and in b, $P_c$ at the base of the pH 6.8 sandbox = 9.1 cm $H_2O$.

At the completion of the low pH experiment, the applied capillary pressure at the base of the iron oxide-coated sand heterogeneity was 8.64 cm water (Fig. 9a). The $P_c$–S curves suggest that effective water saturation would be approximately 45% and 36%, in the iron oxide-coated sand and the quartz sand, respectively (Fig. 7b). These effective water saturations are larger than the observed flow cell saturations (based on LTV and destructive sampling). It should be noted, however, the $P_c$–S curves at the lower pH are relatively flat, with small changes in the capillary pressure resulting in large changes in water saturation. At pH 6.3 the applied capillary pressure at the base of the iron oxide heterogeneity at completion was 6.4 cm water; this corresponds to effective water saturations of 87% and 33% expected in the iron oxide-coated sand and quartz sand, respectively, based on the $P_c$–S curves (Fig. 7a). As discussed earlier, water in the quartz sand was completely displaced by PCE consistent with the expected effective water saturation based on the $P_c$–S curves. On the other hand, no PCE was observed in the iron oxide-coated sand at the completion of the experiment, whereas the $P_c$–S curves would suggest a relatively small amount of PCE in the iron oxide-coated heterogeneity. However, the van Genuchten model, embedded in the multistep outflow approach employed to derive the $P_c$–S relationships, does not predict a distinct entry pressure even when homogeneous sands of this nature are known to exhibit distinct entry pressures in multiphase flow experiments (e.g., Gerhard and Kueper, 2003a). Use of a Brooks–Corey type $P_c$–S curve, with a distinct entry pressure, in the multistep outflow approach may yield an effective water saturation of 1.0 at this imposed capillary pressure. Further increases in capillary pressure were not possible in either experiment as PCE began to exit

the flow cell once it had reached the upper boundary. As such, it was not possible to quantify the applied capillary pressure at which PCE would invade the iron oxide-coated sand at pH 6.3. Results from the flow cell experiments are consistent with the intrinsic contact angle and $P_c$–S curves suggesting that wettability alterations can be induced by the surfactants with significant implications for the distribution of NAPLs at contaminated sites.

## 4. Summary and conclusion

This study suggests that minerals present on the soil surface could have important implications related to multiphase flow predictions used for contaminated site remediation. At the scale of a single drop, an iron oxide surface remained hydrophilic in the pH range $3.5 < pH < 7.5$, whereas a quartz surface, while also hydrophilic at low pH values, exhibited strong NAPL-wetting behavior at near-neutral pH values with DDA. Hysteresis in contact angle was observed for both quartz and iron oxide surfaces. However, at neutral pH the iron oxide surface exhibited larger than expected hysteresis, remaining strongly hydrophilic as the droplet advanced but switching to strongly hydrophobic as the PCE droplet receded. Capillary pressure–saturation experiments with quartz and iron oxide-coated sands revealed that intrinsic contact angle similarities at low pH and intrinsic contact angle differences at near-neutral pH were both reflected in the REV-scale $P_c$–S relationship. Furthermore, the influence of these wettability effects on macroscopic DNAPL invasion in a heterogeneous flow cell was confirmed. At pH 6.8, under identical boundary capillary pressures, PCE entered and displaced the majority of water in the quartz sand but did not enter the iron oxide-coated sand heterogeneity. In addition, the significant hysteresis present on iron oxide surfaces at neutral pH suggest that while water drainage behavior for quartz and iron oxide sands may be different, water imbibition behavior may be similar.

Experiments performed in this study highlight the significant effect that mineral isoelectric points may have on NAPL wettability in the presence of surface active chemicals. While this study focused on examining the differences between quartz and iron oxide surfaces, similar non-ideal behavior is expected when charged surfactants, often present upon disposal of NAPL wastes, are present in NAPL mixtures and encounter subsurface minerals corresponding to a wide range of isoelectric points. Furthermore, this study focused on a positively charged organic base (DDA); however anionic surfactants were frequently employed in NAPL mixtures for a variety of applications. As such, it is likely that negatively charged anionic surfactants will sorb to positively charged mineral solids in the subsurface, potentially altering the wettability.

Simplifying assumptions were employed in this study such as the use of: uniform, homogeneous soil types free from organic carbon, reagent grade chemicals, a chemically pure aqueous phase, monovalent salts and iron oxide coatings which may be different from iron oxides found in the field. Nevertheless, the conclusions made in this study with regard to the role of the solid's isoelectric point in determining NAPL/surfactant/water wettability are expected to be applicable to real subsurface systems containing a broad range of minerals. These real systems may include various minerals in a well mixed fractional wetting system or distinct blocks and layers of minerals as seen in the flow cell experiments.

These results have significant implications for DNAPL distribution in the field, especially at sites such as dry cleaning facilities or waste solvent disposal areas where DNAPL/surfactant mixtures are likely to be found. The distribution of minerals, as well as the site's aqueous pH value, may have a significant impact on the DNAPL source zone architecture. Commonly occurring minerals that exhibit dissimilar isoelectric points from quartz include iron, aluminum and manganese oxides, among others listed in Table 1. Even if a small fraction of soil grains present at a site possess different isoelectric points then the common assumption of homogeneous wetting behavior (either hydrophilic or hydrophobic) should be reconsidered.

## Acknowledgements

This research was supported by the Natural Sciences and Engineering Research Council (NSERC) of Canada through a Strategic Grant and a Canadian Foundation for Innovation Grant.

## References

Abriola, L.M., et al., 2005. Compositional effects on interfacial properties in contaminated systems: implications for organic liquid migration and recovery. In: Berkey, E., Zachry, T. (Eds.), Subsurface Contamination Remediation. American Chemical Society, Washington, D.C., pp. 160–182.

Arye, G., Nadav, I., Chen, Y., 2007. Short-term reestablishment of soil water repellency after wetting: effect on capillary pressure–saturation relationship. Soil Science Society of America Journal 71 (3), 692–702.

Bauters, T.W.J., et al., 2000. Physics of water repellent soils. Journal of Hydrology 231, 233–243.

Birak, P.S., Miller, C.T., 2009. Dense non-aqueous phase liquids at former manufactured gas plants: challenges to modeling and remediation. Journal of Contaminant Hydrology 105 (3–4), 81–98.

Bob, M.M., Brooks, M.C., Mravik, S.C., Wood, A.L., 2008. A modified light transmission visualization method for DNAPL saturation measurements in 2-D models. Advances in Water Resources 31 (5), 727–742.

Bradford, S.A., Phelan, T.J., Abriola, L.M., 2000. Dissolution of residual tetrachloroethylene in fractional wettability porous media: correlation development and application. Journal of Contaminant Hydrology 45 (1–2), 35–61.

Brooks, R.H., Corey, A.T., 1964. Hydraulic properties of porous media. American Society of Agricultural Engineers — Transactions 7 (1), 26–28.

Buckley, J.S., Liu, Y., 1998. Some mechanisms of crude oil/brine/solid interactions. Journal of Petroleum Science and Engineering 20 (3–4), 191–202.

Buckley, J.S., Lord, D.L., 2003. Wettability and morphology of mica surfaces after exposure to crude oil. Journal of Petroleum Science and Technology 39 (3–4), 261–273.

Cornell, R.M., Schwetmann, U., 2003. The Iron Oxides: Structure, Properties, Reactions, Occurrences and Uses. WILEY-VCH Verlag GmbH & Co. KGaA, Weinheim.

Darnault, C.J.G., et al., 1998. Visualization by light transmission of oil and water contents in transient two-phase flow fields. Journal of Contaminant Hydrology 31 (3–4), 337–348.

Demond, A.H., Desai, F.N., Hayes, K.F., 1994. Effect of cationic surfactants on organic liquid–water capillary pressure–saturation relationships. Water Resources Research 30 (2), 333–342.

Desai, F.N., Demond, A.H., Hayes, K.F., 1992. The influence of surfactant sorption on capillary pressure–saturation relationships. Transport and Remediation of Subsurface Contaminants: Colloidal, Interfacial and Surfactant Phenomena. American Chemical Society, Washington, D.C, pp. 133–148.

Dou, W., Omran, K., Grimberg, S.J., Denham, M., Powers, S.E., 2008. Characterization of DNAPL from the US DOE Savannah River Site. Journal of Contaminant Hydrology 97 (1–2), 75–86.

Dwarakanath, V., Jackson, R.E., Pope, G.A., 2002. Influence of wettability on the recovery of NAPLs from alluvium. Environmental Science & Technology 36 (2), 227–231.

Feldman, S.B., Shang, C., Zelazny, L.W., 2008. Soil mineralogy. In: Chesworth, W. (Ed.), Encylopedia of Soil Science. Springer, Dordrecht, pp. 678–685.
Gerhard, J.I., Kueper, B.H., 2003a. Capillary pressure characteristics necessary for simulating DNAPL infiltration, redistribution, and immobilization in saturated porous media. Water Resources Research 39 (8), 1212, 7-1–7-17.
Gerhard, J.I., Kueper, B.H., 2003b. Influence of constitutive model parameters on the predicted migration of DNAPL in heterogeneous porous media. Water Resources Research 39 (10), 1279, 4-1–4-13.
Grant, G.P., Gerhard, J.I., Kueper, B.H., 2007. Multidimensional validation of a numerical model for simulating a DNAPL release in heterogeneous porous media. Journal of Contaminant Hydrology 92 (1–2), 109–128.
Harrold, G., Gooddy, D., Lerner, D.N., Leharne, S.A., 2001. Wettability changes in trichloroethylene-contaminated sandstone. Environmental Science & Technology 35 (7), 1504–1510.
Harrold, G., Lerner, D.N., Leharne, S.A., 2005. The impact of additives found in industrial formulations of TCE on the wettability of sandstone. Journal of Contaminant Hydrology 80 (1–2), 1–17.
Hsu, H.-L., Demond, A.H., 2007. Influence of organic acid and organic base interactions on interfacial properties in NAPL–water systems. Environmental Science & Technology 41 (3), 897–908.
Jackson, R.E., Dwarakanath, V., 1999. Chlorinated degreasing solvents: physical–chemical properties affecting aquifer contamination and remediation. Ground Water Monitoring and Remediation 19 (4), 102–110.
Jeong, S.W., Wood, A.L., Lee, T.R., 2002. Effects of pure and dyed PCE on physical and interfacial properties of remedial solutions. Journal of Hazardous Materials 95 (1–2), 125–135.
Johnson, P.R., Sun, N., Elimelech, M., 1996. Colloid transport in geochemically heterogeneous porous media: modeling and measurements. Environmental Science & Technology 30 (11), 3284–3293.
Lord, D.L., Demond, A.H., Salehzadeh, A., Hayes, K.F., 1997. Influence of organic acid solution chemistry on subsurface transport properties. 2. Capillary pressure–saturation. Environmental Science & Technology 31 (7), 2052–2058.
Lord, D.L., Demond, A.H., Hayes, K.F., 2000. Effects of organic base chemistry on interfacial tension, wettability and capillary pressure in multiphase subsurface waste systems. Transport in Porous Media 38 (1–2), 79–92.
Lord, D.L., Demond, A.H., Hayes, K.F., 2005. Comparison of capillary pressure relationships of organic liquid–water systems containing an organic acid or base. Journal of Contaminant Hydrology 77 (3), 195–208.
Mayer, A.S., Hassanizadeh, S.M., 2005. Soil and Groundwater Contamination: Nonaqueous Phase Liquids. American Geophysical Union, Washington, D.C.
McNeil, J.D., Oldenborger, G.A., Schincariol, R.A., 2006. Quantitative imaging of contaminant distributions in heterogeneous porous media laboratory experiments. Journal of Contaminant Hydrology 84 (1–2), 36–54.
Melrose, J.C., 1965. Wettability as related to capillary action in porous media. Society of Petroleum Engineers — Journal 5 (3), 259–271.
Mercer, J.W., Cohen, R.M., 1990. A review of immiscible fluids in the subsurface: properties, models, characterization and remediation. Journal of Contaminant Hydrology 6 (2), 107–163.
Morrow, N.R., 1975. The effects of surface roughness on contact angle with special reference to petroleum recovery. Journal of Canadian Petroleum Technology 14 (4), 42–53.
Murray, M.D., Darvell, B.W., 1990. A protocol for contact-angle measurement. Journal of Physics. D. Applied Physics 23 (9), 1150–1155.
National Research Council, 2005. Contaminants in the Subsurface: Source Zone Assessment and Remediation. The National Academies Press, Washington D.C.
Nellis, S.R., Yoon, H., Werth, C.J., Oostrom, M., Valocchi, A.J., 2009. Surface and interfacial properties of nonaqueous-phase liquid mixtures released to the subsurface at the Hanford Site. Vadose Zone Journal 8 (2), 343–351.
Niemet, M.R., Selker, J.S., 2001. A new method for quantification of liquid saturation in 2D translucent porous media systems using light transmission. Advances in Water Resources 24 (6), 651–666.
O'Carroll, D.M., Sleep, B.E., 2007. Hot water flushing for immiscible displacement of a viscous NAPL. Journal of Contaminant Hydrology 91 (3–4), 247–266.
O'Carroll, D.M., Bradford, S.A., Abriola, L.M., 2004. Infiltration of PCE in a system containing spatial wettability variations. Journal of Contaminant Hydrology 73 (1–4), 39–63.
O'Carroll, D.M., Abriola, L.M., Polityka, C.A., Bradford, S.A., Demond, A.H., 2005a. Prediction of two-phase capillary pressure–saturation relationships in fractional wettability systems. Journal of Contaminant Hydrology 77 (4), 247–270.
O'Carroll, D.M., Phelan, T.J., Abriola, L.M., 2005b. Exploring dynamic effects in capillary pressure in multistep outflow experiments. Water Resources Research 41 (11), W11419, 1–14.
Parks, G., 1965. The isoelectric points of solid oxides, solid hydroxides, and aqueous hydroxo complex systems. Chemical Reviews 65 (2), 177–198.
Powers, S.E., Tamblin, M.E., 1995. Wettability of porous-media after exposure to synthetic gasolines. Journal of Contaminant Hydrology 19 (2), 105–125.
Powers, S.E., Anckner, W.H., Seacord, T.H., 1996. Wettability of NAPL-contaminated sands. Journal of Environmental Engineering 122 (10), 889–896.
Roy, J.L., McGill, W.B., 1998. Characterization of disaggregated nonwettable surface soils found at old crude oil spill sites. Canadian Journal of Soil Science 78 (2), 331–344.
Ryder, J., Demond, A., 2008. Wettability hysteresis and its implications for DNAPL source zone distribution. Journal of Contaminant Hydrology 102 (1–2), 39–48.
Sghaier, N., Prat, M., Ben Nasrallah, S., 2006. On the influence of sodium chloride concentration on equilibrium contact angle. Chemical Engineering Journal 122 (1–2), 47–53.
Singh, U., Uehara, G., 1999. Electrochemistry of the double layer: principles and applications to soils. Soil Physical Chemistry. CRC Press, Boca Raton, pp. 1–46.
Sposito, G., 1989. The Chemistry of Soils. Oxford University Press, New York.
Stokes, M., Anderson, M., Chandrasekar, S., Motta, R., 1996. A standard default color space for the internet — sRGB. World Wide Web Consortium, p. 1.
Thomas, M.M., Clouse, J.A., Longo, J.M., 1993. Adsorption of organic compounds on carbonate minerals. 1. Model compounds and their influence on mineral wettability. Chemical Geology 109 (1–4), 201–213.
Tuck, D.M., Iversen, G.M., Pirkle, W.A., 2003. Organic dye effects on dense nonaqueous phase liquids (DNAPL) entry pressure in water saturated porous media. Water Resources Research 39 (8), 1207, 5-1–5-13.
van Genuchten, M.T., 1980. Closed-form equation for predicting the hydraulic conductivity of unsaturated soils. Soil Science Society of America Journal 44 (5), 892–898.
Wang, H.G., Chen, X.S., Jawitz, J.W., 2008. Locally-calibrated light transmission visualization methods to quantify nonaqueous phase liquid mass in porous media. Journal of Contaminant Hydrology 102 (1–2), 29–38.
Yoon, H., Oostrom, M., Werth, C.J., 2009. Estimation of interfacial tension between organic liquid mixtures and water. Environmental Science & Technology 43 (20), 7754–7761.
Zheng, J., Powers, S.E., 1999. Organic bases in NAPLs and their impact on wettability. Journal of Contaminant Hydrology 39 (1–2), 161–181.
Zheng, J., Shao, J., Powers, S.E., 2001. Asphaltenes from coal tar and creosote: their role in reversing the wettability of aquifer systems. Journal of Colloid and Interface Science 244 (2), 365–371.